High-temperature deformation followed in situ by X-ray microtomography: a methodology to track features under large strain

Pierre Lhuissier, Therese Bormann, Guillaume Pelloux, Xavier Bataillon, Franck Pelloux, Charles Josserond, Pauline Gravier, Jean-Jacques Blandin, Elodie Boller, Luc Salvo

manuscript t115523 for review

JOURNAL OF SYNCHROTRON RADIATION

High temperature deformation followed in situ by X-ray micro-tomography: A methodology to track features under large strain

Pierre Lhuissier, Therese Bormann, Guillaume Pelloux, Xavier Bataillon, Franck Pelloux, Charles Josserond, Pauline Gravier, Jean-Jacques Blandin, Elodie Boller and Luc Salvo

Category: *research papers*

Co-editor:

Telephone:

Fax:

Email:

Submitting author:

Pierre Lhuissier

Univ. Grenoble Alpes, CNRS, Grenoble INP, SIMAP, , F-38000 , Grenoble, France

Telephone: +33476826342

Fax: +33476826382

Email: pierre.lhuissier@simap.grenoble-inp.fr

High temperature deformation followed in situ by X-ray micro-tomography: A methodology to track features under large strain

Lhuissier Pierre,[a]* Bormann Therese,[a] Pelloux Guillaume,[a]
Bataillon Xavier,[a] Pelloux Franck,[a] Josserond Charles,[a]
Gravier Pauline,[a] Blandin Jean-Jacques,[a] Boller Elodie[b] and
Salvo Luc[a]

[a] *Univ. Grenoble Alpes, CNRS, Grenoble INP, SIMAP, F-38000 Grenoble, France, and* [b] *ID19 beamline - ESRF, 6 rue Jules Horowitz, BP 220, 38043 Grenoble Cedex 9, France.*

E-mail: pierre.lhuissier@simap.grenoble-inp.fr

Abstract

Metallic materials processing such as rolling, extrusion or forging, often involves high temperature deformation. Usually in such conditions samples are characterized in *post-mortem* conditions, in pseudo *in situ* condition with interrupted tests or *in situ* with limited strain rate. A full *in situ* 3D characterization, namely directly during high temperature deformation with a prescribed strain rate scheme, requires a dedicated sample environment and a dedicated image analysis workflow. A specific sample environment has been developed to be able to conduct highly controlled (temperature and strain rate) high temperature deformation mechanical testing while performing in situ

tomography on a synchrotron beamline. A dedicated digital volume correlation algorithm is used to estimate the strain field and track pores while the material endures large deformations. The algorithm is particularly suitable for materials with few internal features when deformation steps between two images are large. An example of application is provided : high temperature compression test on a porous aluminum alloy with individual pore tracking with a specific strain rate scheme representative of rolling conditions.

1. Introduction

Processing of metallic materials often requires high temperature deformation (forging, rolling...). In such high temperature conditions, the mechanical behaviour of the materials can be highly sensitive to the applied strain rate (visco-plastic regime). Some deformation mechanisms are thermally activated and thus present a time dependency. The strain rate cannot be varied arbitrary without potentially changing the predominant deformation mechanisms (dislocation glide, dislocation creep, diffusion, grain boundary sliding...). During constant strain rate tests, any interruption of straining in order to perform an X-ray tomography scan is clearly detrimental, since it can induce an important bias in the identification of the observed mechanisms. Thus, it is mandatory to be able to image the sample during straining without any change of both the strain rate and temperature. This often comes with large strain increments between 3D images due to the constrains of data flow and memory size of the camera. Similarly, when the strain rate scheme is more complex, the tomography scans are preferentially performed during low strain rate segments and results in large strain increments. The strain rate constrain also implies a trade-off on the acquisition time : long exposure time and large number of projections reduce noize but increase potential bluring due to sample drift, deformation and internal features evolution. While some

regularisation can be applied to correct sample drift and sample straining (Jailin & Roux, 2018), internal feature evolution, whose evolution characterization is generally the purpose of the test, are hardly predicted. As a consequence, one might need to significantly reduce acquisition time and thus images quality during high temperature deformation test.

In the present experiment, a loading device able to control with a high accuracy displacement and strain rate on millimetric specimens, both in tension and compression has been developed. The system is designed to allow high temperature deformation with a fine temperature control. The overall system is compatible with fast *in situ* micro tomography, meaning that it is compatible with scanning time of less than a few seconds with a micrometric resolution. A specific work flow for data analysis has also been developed in order to estimate the strain field and to ensure automatic tracking of features of interest such as particles or pores. A specific Digital Volume Correlation (DVC) procedure has been implemented in order to handle large deformations between two images and weak images texture. Features of interest are then automatically tracked and analyzed even when they are highly changing (such as pore nucleation, pore closure, pore coalescence). Classical images analysis procedures can then easily be applied to estimate morphological evolutions.

2. Experiment

High temperature deformation requires the combination of a loading device and a heating system. The present device has been designed in order to allow continuous rotation on the tomography rotating stage. It consists in a loading system (actuator and sensor) coupled with a specific sample holder, compatible with several heating devices. The loading device stands on the rotating stage and thus turns continuously during X-ray micro-tomography acquisitions, while the furnace is fixed.

2.1. Heating systems

Depending on the testing temperature several heating devices can been used.
For tests up to $800°C$, a resistive furnace is used. The furnace has been developed by AET several years ago, see (Limodin *et al.*, 2009) for more details. Its main characteristics are a maximal temperature of $800°C$ with a maximal heating rate of about $1°C/s$. This furnace has two glassy carbon windows to allow the X-ray beam to go through. The furnace is placed on a so called "camera manipulator" over the rotating stage and accurately aligned with the center of rotation. A motor allows the furnace to move down to heat the sample. While in down position, the sample is in the furnace, the X-ray beam goes through the glassy carbon windows and through the sample, and the sample can rotate freely around the vertical axis (tomographic rotation axis). A small horizontal translation of the sample (few millimeters) inside the furnace is possible in order to move the sample out of the field of view and record reference images (also called "flat field").
The furnace temperature and ramp rate are controlled in a dedicated SPEC session using a Eurotherm interface. Motors controlling the furnace motion are also integrated to the main SPEC session. Furnace temperature is recorded by SPEC and can also be used to trigger an experiment.

For temperatures higher than $800°C$ an inductive heating is used. It consists in a Hüttinger TIG5/300 system (rated power of 5kW, adjustable coupling frequency from 30 to 300kHz) with an in-house water cooled copper coil. The coil axis is parallel to the rotation axis. A space between the coils allows a shadow free path for the X-ray beam. Temperature is measured directly in the region of interest of the sample thanks to a fiber optic bi-chromatic Impac IGAR 12-LO pyrometer (spectral lengths : $1.52\mu m/1.64\mu m$, adjustable optic from 200 to 350 mm corresponding to a measuring

spot diameter from 0.8 to 1.5 mm). The temperature is then manually monitored in order to avoid any instability. The power is manually adjusted with 0.1% accuracy.

The temperature of the sample is accurately calibrated using an original procedure relying on direct imaging. Actually, the system is too complex for a fine preliminary calibration. Indeed X-ray beam can induce some heating, the sample holder, the sample geometry, the grips and the sample position might change the temperature field. Thus an experimental calibration is performed every time the setup is installed on the beamline. Samples made of predefined eutectic compositions allow to measure accurately some specific temperatures. For these eutectic compositions, by definition, the liquidus and solidus become mixed up. The material changes from fully liquid to fully solid at a well known temperature. It is not sensitive to a small change in the eutectic composition. Depending on the temperature range of the tests, different eutectic are used : $Sn9wt\%Zn$ ($198°C$), $Al54wt\%Ge$ ($424°C$), $Al33wt\%Cu$ ($548°C$), $Al6.1wt\%Ni$ ($640°C$), $Cu30wt\%Si$ ($802°C$), $Ni71.6wt\%Ti$ ($942°C$), $Cu9wt\%Zr$ ($980°C$), $Ni51.9wt\%Nb$ ($1175°C$) or $Ni23.2wt\%Nb$ ($1282°C$). The required furnace temperature to reach the targeted sample temperature is then determined by linear interpolation. In such a way, the temperature of the sample is accurately controlled.

2.2. Loading device

The loading device is composed of a moto-reductor, gears, an endless screw, a moving cross tie, a load sensor and specific sample holders.
Figure 1a presents the overall system composed of the tensile device in room temperature configuration and of the controller. Figure 1b presents the system integrated on ID19 ESRF beamline in the high temperature condition with the furnace in upper

position. Figure 1c presents a 2D cross section of the CAD of the loading device.

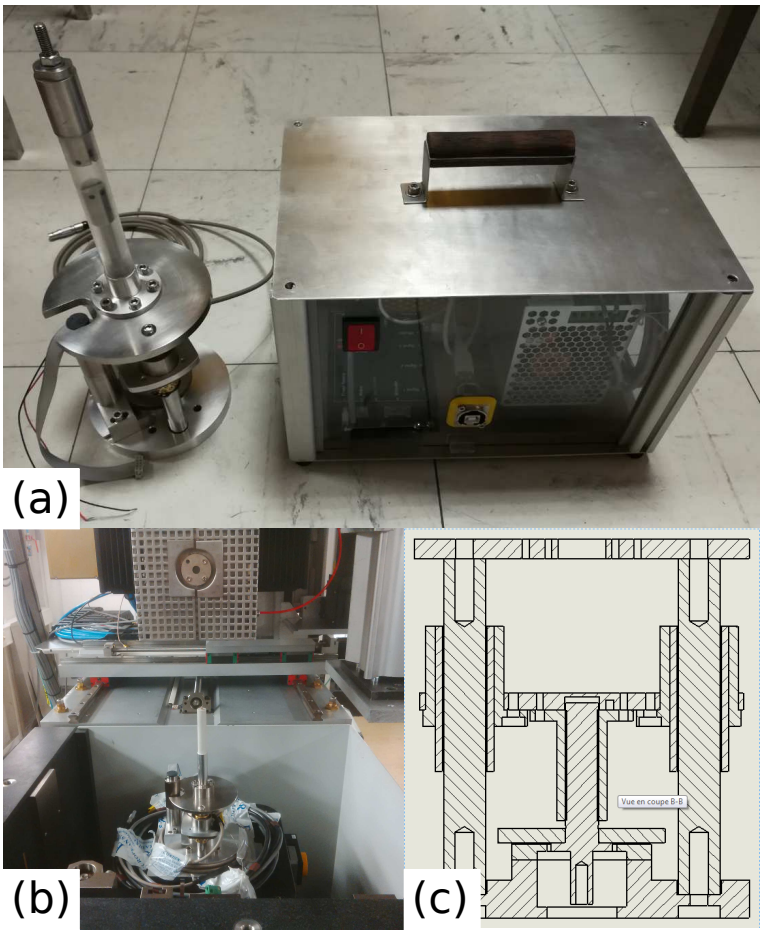

Fig. 1. **(a)** Complete system composed of the controller and of the tensile system in room temperature configuration. **(b)** Overall system integrated on ID19 ESRF beamline with the furnace in upper position. **(c)** 2D cross section of the loading device.

Motion is ensure thanks to Maxon DC moto-reductors. A DCX 22L GB KL 36V motor was selected. Two GPX22 C reductors are available : ratio 150:1 and ratio 35:1. The motor is equipped with a 1024 steps encoder. A gear is screwed on the moto-reductor axis. Depending on the desired experimental conditions, the gear holds 38 or 55 tooth. It is connected to a 120 tooth gear sealed to the endless screw. Gears hold 0.5mm tooth and are made of varied steel quality depending on the required maximal

load. All gears comes from HPC company. The endless screw rotates around a vertical axis thanks to a pre-strained ball bearing BEAS 008032-2RS from SKF. The endless screw is connected to a specific nut. Both have been machined on purpose. The nut is connected to the moving cross-tie. The cross-tie is guided thanks to 2 ball sleeves (7631.015, 7301.15 and 6541.015 from Economax). On the cross-tie stands a load cell. Depending on the required maximal load, a 20N, 50N, 200N, 500N, 2kN or 5kN load cell can be used (series 8523 and 8524 from Burster). The load signal is amplified and converted to a 4-20mA signal by APJ-OEM from TEM. Signal is then converted to a 2-10V signal by a 500Ω resistor and recorded by an analog usb module (USB-1408FS from Measurment computing). The complete chain is calibrated on a laboratory tension/compression mechanical device (DY24 from ADAMEL) with a suitable load cell (calibrated every year by a certified company). A thermocouple transmitter from TC direct converts the signal of a K or a S thermocouple to a 4-20mA current. The analog usb module records the 2-10V tension at the edges of a 500Ω resistor.

The moto-reductor control is ensured by an EPOS 2 motor controller. Specific connectors are wired in order to make all the signal going through the slip ring of the ESRF ID19 beamline rotating stage. Thus the system can turn *ad nauseam*.

The user interface is an in house GUI based on Qt and proprietary Linux libraries. It enables to display data, to control the motor (position, velocity, strain rate, limits...) and to store data. The software is installed on a Raspberry Pi 2.

Two compatible versions of the device exist. Table 1 summarizes the mains characteristics of the two versions.

Table 1. *Main characteristics of the two versions of the loading device.*

Maximal stroke	$10mm$	$25mm$
Maximal load	$2kN$	$5kN$
Minimal velocity	$1.310^{-2}\mu m/s$	$2.610^{-2}\mu m/s$
Maximal velocity	$1.010^{3}\mu m/s$	$2.010^{3}\mu m/s$
Overall height	$86mm$	$110mm$

2.3. Beamline integration

The system is integrated on the ID19 beamline at the ESRF. The loading system stands on a Leuven rotating stage. All signals go through a slip ring integrated inside the rotating stage. Data have been reconstructed using ESRF fasttomo3 pre-processing and PyHST2 (Mirone *et al.*, 2014). Post-reconstruction ring removal has been conducted using an in house ESRF matlab code (Lyckegaard *et al.*, 2011). Data have been cropped and converted to 8bits using fixed ROI and range per sample. Post-processing has been conducted using ImageJ (Schneider *et al.*, 2012) and in house plugins (Boulos *et al.*, 2012).

2.4. Digital Volume Correlation

A dedicated Digital Volume Correlation (DVC) algorithm is implemented to deal with the specificities of such high temperature tests, namely large deformation between two images, heterogeneous strain field and weak texture of images.
The correlation is performed in several steps. The principle of the algorithm is illustrated in Figure 2

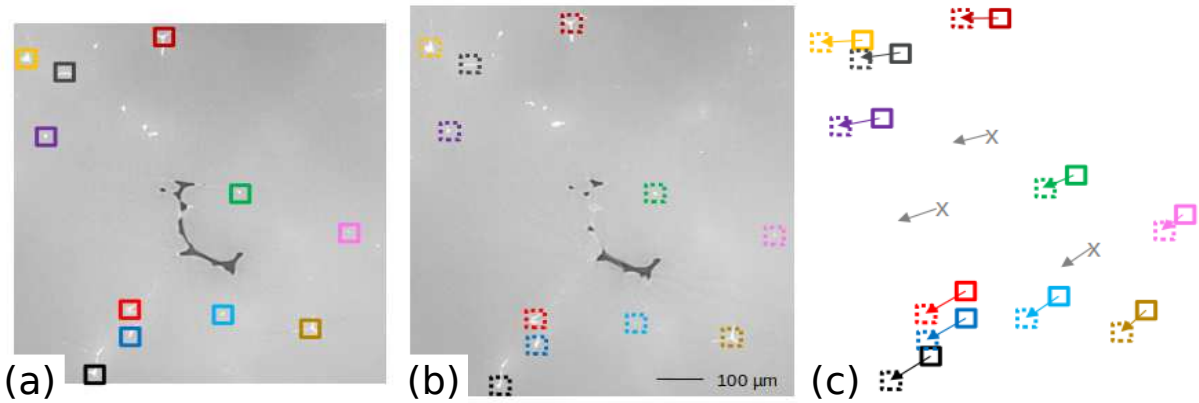

Fig. 2. Principle of the DVC algorithm. Feature are detected and tracked from the reference state **(a)** to the deformed state **(b)** in order to get an estimation of the displacement field in any point by interpolation : grey crosses in **(c)**.

First, features used for subsequent tracking are identified. Such features must be robust with respect to the cross correlation algorithm. In other words, it means that these features have to exhibit "large grey level gradients" in all directions as well as small changes of shape from one stage to the other. The identification of theses features is based on a 3D Harris' corner detection algorithm (Harris & Stephens, 1988) with a mask on possible location of the points and imposed minimal distance between selected points. The features are usually intermetallic second phase particles which seldomly evolve from one image to the other. This initial set of points can be reduced depending on a region of interest. This set will be labelled *"guiding points"*. These guiding points are ordered based on the quality of the pattern. The larger is the Harris' corner value (ie the absolute value of the smallest eigenvalue of the second moment matrix also called autocorrelation matrix), the higher is the pattern quality for a tracking purpose.

The guiding points are tracked from an image (labelled *"initial image"*) to the next one (labelled *"final image"*) in an iterative procedure. It relies on the cross correlation of a small parallelepipedic window (usually between 10 and 20 voxel in each dimension) centered on a guiding point in the initial image and the same parallelepipedic window translated (in the 3 dimensions) in the final image. The cross correlation used here is a normalized cross correlation corrected from the average intensity in each image (as suggested in (Doumalin, 2000)). The best cross correlation coefficient is stored and used to define the matching position. If required a rigid motion in rotation can also be applied. Nevertheless these additional degrees of freedom are usually not used for computation cost-efficiency. It seldom improves the accuracy of the results (at least for the specific materials and tests conducted in the present work). The guiding points are looked for in the final image within a *"research window"* around a *"guessed position"*. The research window is usually anisotropic in order to match the maximal

local motions which are larger in the tensile/compression direction. The size of the research window is of several tens of voxels in each direction (usually about 50-80 in tensile/compression direction and about 20-30 in the transverse direction). The research window of the first guiding point is enlarged by a factor 5 to 8. This first point is searched in the final image around a guessed position which is equal to its position in the initial image. All other guiding points are sorted in a queue depending on their distance to any point of the queue (i.e. the point the closest to any point of the queue is the next one to be en-queued). Then the queue is processed. For each point, a guessed position in the final image is estimated. The guessed position is based on a weighted average of the position of some guiding points already tracked. The average uses only points located within a given distance of the currently processed point in the initial image whose already performed correlation factor is higher than a threshold. The average is weighted by a gaussian of the distance. After processing the whole guiding points queue, a first estimate of the position of the guiding points in the final image is available, and the quality of each tracking is assessed based on the correlation coefficient.

Then a second iteration of tracking is performed after some regularization. The regularization consists in the identification of inconsistent positions. It is a direct implementation of the coherency estimation algorithm of (Masullo & Theunissen, 2016). The original algorithm has been developed for Particle Image Velocimetry (PIV) and is efficient for such heterogeneous displacement fields.

Guiding points within a given distance of the point of interest in the original image and with a correlation coefficient higher than a threshold are used to estimate the position of the point of interest in the final image. The position is estimated thanks to a quadratic fit of the displacement between initial and final images. If the position found during the first correlation iteration is close to the fit then the point is consid-

ered as valid (the correlated factor is kept unchanged). Otherwise it is considered as badly correlated (the correlated factor is set to zero). All points are processed. Then the regularization algorithm is run a second time to define the guessed position (thus badly correlated points are not accounted for to determine the guessed position). The cross correlation is then performed on all the guiding points queue using these guessed positions and a reduced research window (usually the initial one divided by a factor 2 to 4). Positions of the guiding points in the final image and the last correlation factor are stored.

The guiding points are then used to estimate the strain field and to track feature of interest.

A mesh of 8 noded bricks is defined over the region of interest. The displacement of each of the node is estimated based on a quadratic fit of the displacement of nearby guiding points with a sufficiently high correlation factor. A deformed mesh is thus defined. Initial and deformed meshes are then processed by a finite element code Cast3M (Cast3M, 2019) in order to compute local strain fields. Stress fields can also be computed with the same finite element code using some of the experimental displacement as boundary conditions. However it obviously requires to provide as input a constitutive law. Note that with this implementation there is no optimization of the parameters of the constitutive law.

Virtual position of features of interest in any images can be estimated using a similar quadratic fit on guiding points. It enables to link features from one image to another, for example by using the label of the closest feature from the virtual position either based on a features list or directly on a labelled image. Thus it enables to follow features evolution even when objects are complex and/or elongated and split or merge.

The DVC and tracking procedure is implemented in C++ and CUDA in order to run

on GPGPU and benefits from the high degree of parallelism of the computation. The overall procedure lasts a couple of hours. Table 2 gives an example of computational time for a dataset. All outputs are written to vtk format in order to be visualized with Paraview (Ahrens *et al.*, 2005).

Table 2. *Example of computational time for a given data-set.*

Number of 3D images	8
Size of 3D images [voxels]	1000x1000x670
Strain increment between images	5-20%
Number of guiding points	4600
Pattern window size [voxels]	11x11x11
Research window size [voxels]	41x41x101
Initial point research window size [voxels]	161x161x401
Number of mesh cells	10x10x20
Number of tracked objects	$\approx$ 300
Processors	Intel Xeon E5-2605v3 @1.90GHz
Number of processors	2
Number of core per processor	6
GPU	Quadro K4200
Average total time	2h30

2.5. Materials and tests

A single example is presented here : the high temperature compression of an as-cast 2050 aluminum alloy sample presenting large solidification pores. A specific strain rate scheme was applied to mimic rolling scheme : a succession of high strain rate segments and holding time. Cylindrical samples with a diameter of 2mm and a height of 2mm have been compressed at $480°C$ with alternated relatively high strain rate steps (about $1s^{-1}$ over $200\mu m$ die displacement, meaning roughly 10% strain steps) and 1 minute holding time. The sample is placed in a boron nitride bell and compressed between two inconel dies. A 34keV X-ray beam illuminates the sample. Data are recorded with a PCO-edge detector coupled to a 100 m thick YAG scintillator with a $\times 5$ optic. 2000 radiographs of 1536×1440 pixels are recorded for each scan in 10 seconds between each compression step, while keeping the sample in the furnace.

3. Results and discussion

The proposed example aimed at identifying a criterion for pore closure during high temperature compression. The determination of the displacement field is mandatory to get the local stress field. The large deformation endured by the sample between two images requires a robust algorithm. The displacement field is also required to connect the pores from one time step to the other. The device and the tracking procedure proved to be efficient. The intermetallic chosen as guiding points are branched and relatively homogeneously distributed in the sample. This set of guiding points is thus robust and dense enough to estimate the displacement field in the whole sample. Figure 3 presents an overview of the analysis performed on a sample : 3D pores view, strain field and the relationship between the volume of a given pore and the cumulative local strain.

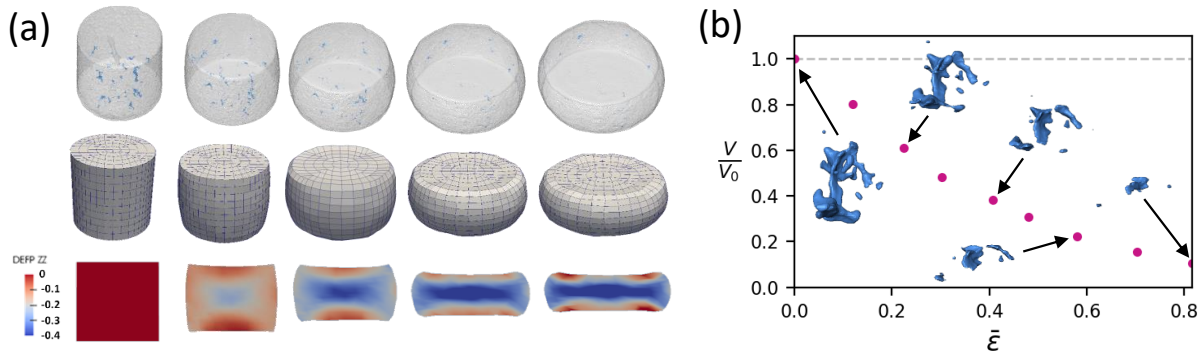

Fig. 3. **(a)** 3D views of the porosity in the sample, mesh deformation measured by DVC and associated strain field (ε_{zz} component)in a vertical cross section for all the compression steps. **(b)** Evolution of the volume of a single pore as a function of the cumulative local strain.

The mesh obtained by DVC is consistent with the sample geometry changes. The strain field appears also consistent with the applied loading. The displacement field

allowed to accurately predict the pores positions from one time step to the other. The tracking thus enabled to plot the evolution of a pore relative volume change as a function of the local strain field as well as the integral of stress triaxiality. The validity of such a criterion for pore closure prediction can thus be investigated.

4. Conclusions

A versatile tension/compression device has been developed. The device is compatible with the constraints of fast synchrotron X-ray micro-tomography and with fine thermal control required for high temperature tests. A specific Digital Volume Correlation (DVC) algorithm has been set up and efficiently implemented in order to make it suitable for handle *in situ* synchrotron high temperature tests that lead to reduced image quality due to high acquisition rate, weak images texture, large deformations, heterogeneous strain field, and potential huge datasets. The device has been validated based on a wide variety of high temperature deformation tests. The DVC procedure has been applied on aluminum samples presenting a weak image texture with large deformation between two steps. The obtained displacement field was reliable since it allowed to track pores during the process. The application of the displacement field as boundaries conditions for Finite Element simulations gave access to the local stress field. These informations can easily be gathered to follow, for a given porosity, morphological parameters such as pore volume and aspect ratio as a function of strain or stress components. The versatility of the system allows to easily expand the current field of investigation. For example, it can be implemented into an X-ray laboratory source to perform room temperature mechanical tests. Acquisition conditions can be optimized for each type of sample by selecting a suitable bell. The DVC procedure was successfully applied to a wide range of acquisitions : in situ nanotomography high temperature tensile tests (Kumar *et al.*, 2019), in situ micro CT firn densification

(Burr, 2017), in situ unfolding of corrugated struts produced by additive manufacturing (Suard *et al.*, 2020).

Acknowledgements

The European Radiation Synchrotron Facility (ESRF) is acknowledged for the long term project MA1876 "Use of coherency and large field of view for fast in situ multi-resolution imaging" and for the MA3484 beamtimes. The french research national agency (ANR) is acknowledged for the post-doctoral grant of Therese Bormann in the framework of EDDAM project. C-TEC/Constellium is acknowledged for the funding of Pauline Gravier PhD.

References

Ahrens, J., Geveci, B. & Law, C. (2005). *Paraview: An end-user tool for large data visualization*, vol. 717. Elsevier München, the visualization handbook ed.

Boulos, V., Fristot, V., Houzet, D., Salvo, L. & Lhuissier, P. (2012). In *DASIP 2012*, p. 6. Karlsruhe, Germany.

Burr, A. (2017). *Investigation of pore closure during polar firn densification*. Ph.D. thesis, Univ. Grenoble Alpes.

Cast3M, (2019). Cast3M, http://www-cast3m.cea.fr/.

Doumalin, P. (2000). *Microextensométrie locale par corrélation d'images numériques*. Ph.D. thesis, Ecole Polytechnique X.

Harris, C. & Stephens, M. (1988). In *Procedings of the Alvey Vision Conference 1988*, pp. 23.1–23.6. Manchester: Alvey Vision Club.

Jailin, C. & Roux, S. (2018). *Materials*, **11**(8), 1395.

Kumar, R., Villanova, J., Lhuissier, P. & Salvo, L. (2019). *Acta Materialia*, **166**, 18–27.

Limodin, N., Salvo, L., Boller, E., Suéry, M., Felberbaum, M., Gailliègue, S. & Madi, K. (2009). *Acta Materialia*, **57**(7), 2300–2310.

Lyckegaard, A., Johnson, G. & Tafforeau, P. (2011). *International Journal of Tomography & Statistics*, **18**(F11), 10.

Masullo, A. & Theunissen, R. (2016). *Experiments in Fluids*, **57**(3).

Mirone, A., Brun, E., Gouillart, E., Tafforeau, P. & Kieffer, J. (2014). *Nuclear Instruments and Methods in Physics Research Section B: Beam Interactions with Materials and Atoms*, **324**, 41–48.

Schneider, C. A., Rasband, W. S. & Eliceiri, K. W. (2012). *Nature Methods*, **9**(7), 671–675.

Suard, M., Plancher, E., Martin, G., Dendievel, R. & Lhuissier, P. (2020). *Advanced Engineering Materials*, **22**(7), 2000315.